The combination of $KMnO_4$ with HMO for cyclic adsorption of heavy metal ions and regeneration of adsorbents

Ruyue Ding, Chao Liu and Fencun Xie

ABSTRACT

In this experiment, three kinds of hydrous manganese dioxide (HMO) with different Zeta potentials were synthesized, and combined with $KMnO_4$ for deep removal of Pb^{2+}, Cd^{2+} and Ni^{2+}. The competitive adsorption of three heavy metal ions was also investigated. The results indicated that the stronger the acidity, the higher the Zeta potential (-54.3) of the synthesized HMO. After regenerating HMO with acidic $KMnO_4$ as eluent, the removal rates of Pb^{2+}, Cd^{2+} and Ni^{2+} could still reach 79.25%, 80.13% and 60.43% after five cycles of adsorption. The promoting mechanism of $KMnO_4$'s effect on HMO was analyzed by SEM, TEM, EDS, FTIR, XRD, XPS, BET, and UV-vis. After absorbing heavy metal ions, HMO will release part of Mn (II), and the released Mn (II) reacts with $KMnO_4$ to form a small amount of highly active in-situ HMO. The 'HMO + $KMnO_4$' system can not only improve the removal rate of heavy metal ions by HMO, and reduce the amount of adsorbent, but also remove the released Mn (II). Because of its reproducibility, efficiency and simplicity, the research on water purification materials and technologies is of significance.

Key words | competitive adsorption, cyclic adsorption, *in-situ* reaction, regeneration, water chemistry

Ruyue Ding
Chao Liu
Fencun Xie (corresponding author)
School of Chemistry and Chemical Engineering,
South China University of Technology,
Guangzhou 510641,
China
E-mail: *acfchxie@scut.edu.cn*

HIGHLIGHTS

- A novel mesoporous δ-MnO_2 nanoparticle with high Zeta potential, large specific surface area and high hydroxyl content was prepared.
- Low cost, simple preparation and high adsorption capacity.
- Competitive adsorption of heavy metal ions.
- Regeneration and cyclic adsorption of adsorbents.
- Adding $KMnO_4$ can greatly improve the removal efficiency of heavy metals and remove the residual Mn (II) in the solution.

doi: 10.2166/wst.2021.108

GRAPHICAL ABSTRACT

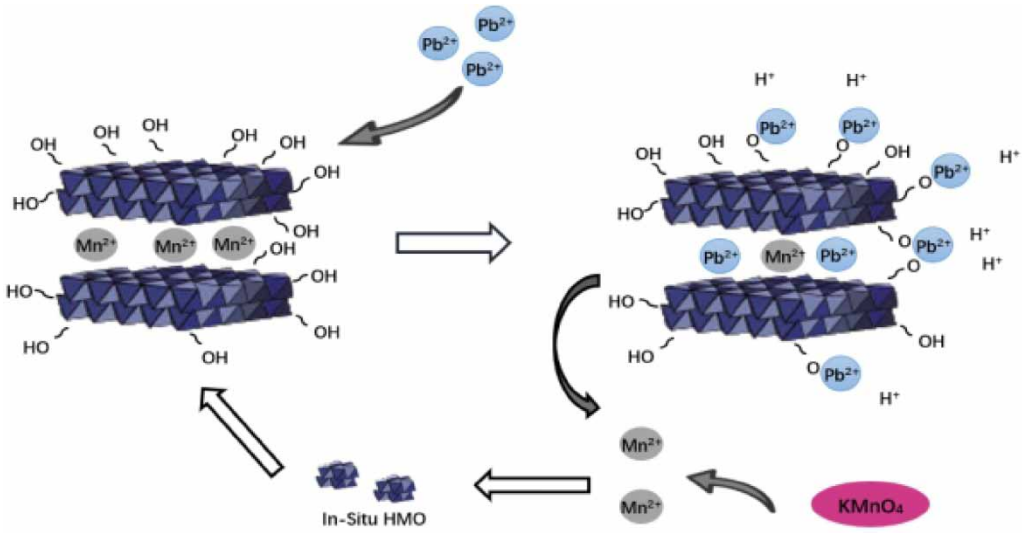

INTRODUCTION

At present, heavy metal ions in soils and the water environment have attracted extensive attention due to strong toxicity, constant bioaccumulation and non-biodegradability (Wongsasuluk *et al.* 2014). Untreated heavy metal wastewater is directly discharged into soil and water bodies, causing severe harm to the entire ecological environment. Therefore, it is extremely urgent to remove heavy metal ions in wastewater to meet the discharge standards. Methods and approaches to remove heavy metal ions have been extensively studied, such as the exchange of ions (Otrembska & Gega 2012), flotation (Patil *et al.* 2016), membrane filtration (Lyu *et al.* 2016), chemical precipitation (Hashim *et al.* 2011), electrochemical treatment (Trellu *et al.* 2016), adsorption (Ojedokun & Bello 2016), and so on. The adsorption method is generally recognized as the most effective method due to its easy operation, low cost, high efficiency and mass production (Sheela *et al.* 2012). There is a variety of mature and developed adsorbents for heavy metal adsorption, including activated carbon (Mezohegyi *et al.* 2012), carbon nanotubes (Sun *et al.* 2014), bio-adsorbents (Gadd 2009), metal oxides (Hua *et al.* 2012), metal-organic frameworks (Li *et al.* 2016) and so on. Although these materials show strong adsorption ability, their complex synthesis process and expensive cost make them impossible to apply in industrial wastewater. Hydrous manganese dioxide (HMO), as a cheap, readily available metal oxide adsorbent with huge adsorption capacity, has a broad application prospect in water treatment (Su *et al.* 2010). Compared with other composite manganese dioxide materials, the freshly synthesized HMO with $KMnO_4$ and H_2O_2 has better adsorption performance for Cd^{2+} (Zhai & Wang 2016). In comparison with other expensive polymeric exchangers, HMO synthesized by the redox reaction of $MnSO_4$ and NaOCl also exhibited a preferable adsorption effect on toxic substances in the presence of Ca^{2+} (Su *et al.* 2010). Nanosized HMO was impregnated on porous polystyrene exchange resin to synthesize HMO-loaded materials to adsorb Pb^{2+} in aqueous solution (Su *et al.* 2009). However, their HMO adsorbents suffer from relatively low adsorption capacity, long adsorption equilibrium time and the HMO-loaded adsorbents will inevitably bring more heavy metal bearing residues. At the same time, the surface of the adsorbent will gradually absorb a large number of impurities during the adsorption process. It will eventually be discarded because it could not meet the water quality requirements. Since the pollutants are only transferred to the adsorbent, they will not be wholly degraded or converted into harmless substances. These waste adsorbents are bound to cause waste of resources and secondary pollution. Therefore, the desorption and regeneration of the adsorbent are of great significance in realizing the recycling of the adsorbent.

In this experiment, three mesoporous materials with different Zeta potentials, δ- MnO_2, were synthesized with

$MnSO_4{\cdot}H_2O$ and $KMnO_4$ as raw materials through a simple and inexpensive redox process at room temperature and low pH conditions. The combination with $KMnO_4$ allowed HMO to show an excellent removal performance for Pb^{2+}, Cd^{2+} and Ni^{2+} in aqueous solution, superior to sole HMO adsorption. Such a combination can not only completely remove heavy metal ions, but also significantly reduces the amount of adsorbent used. The structure of HMO, the adsorption behavior and the promotion mechanism of $KMnO_4$ have been thoroughly studied by a series of experiments and characterizations. The competitive adsorption of Pb^{2+}, Cd^{2+} and Ni^{2+} and the regeneration and cyclic adsorption of the adsorbent were also investigated.

METHODS

Material

This work applied analytical grade chemical reagents from the Damao Chemical Reagent Co., Ltd. Hydrous manganese dioxide was freshly prepared by the titration method of $MnSO_4{\cdot}H_2O$ and $KMnO_4$, and the process can be explained as in Equation (1),

$$3Mn^{2+} + 2MnO_4^- + 2H_2O = 5MnO_2 + 4H^+ \quad (1)$$

0.004 M $KMnO_4$ and 0.004 M $MnSO_4{\cdot}H_2O$ were dissolved in 150 mL deionized water, respectively. Then $MnSO_4{\cdot}H_2O$ was added dropwise to the $KMnO_4$ solution and the mixed solution was stirred with a magnetic agitator at 298.15 K and 150 rpm/min. During the titration, the pH value of the mixed solution should be controlled at 1.5 ± 0.1. Upon completing titration, the current suspension needs to be stirred for another 30 min, and then put aside to settle for 6 h. The suspension needs to be repeatedly flushed with deionized water until the conductivity of the supernatant is less than 2.0 $\eta S{\cdot}cm^{-1}$. The synthetic HMO was prepared into a 100 mL suspension. We synthesized different types of hydrous manganese dioxide (HMO-a, HMO-b, HMO-c) by adjusting the pH ($pH_a = 1.5 \pm 0.1$, $pH_b = 3.5 \pm 0.1$, $pH_c = 5.5 \pm 0.1$) during the reaction process, then they were washed and stored as described above.

We took 1 mL of HMO suspension in a beaker and dissolved it in hydrogen peroxide along with nitric acid. The content of Mn^{2+} in the diluted solution was detected by AAS, then the HMO content was converted into 100 mL of suspension. Pb $(NO_3)_2$, $NiSO_4{\cdot}6H_2O$ and Cd $(NO_3)_2{\cdot}4H_2O$ were respectively dissolved in deionized water to prepare solutions of Pb^{2+}, Ni^{2+} and Cd^{2+}. The 2.0 mmol/L $KMnO_4$ was prepared though the dilution of the standard potassium permanganate solution and then stored in a dark bottle at low temperature.

Characterization

The concentrations of Pb^{2+}, Cd^{2+}, Ni^{2+} and $KMnO_4$ were detected by flame atomic absorption spectrometry (AAS) and UV-Visible spectrometry separately. The sample of crystal structure was comprehensively analyzed with the application of X-ray diffraction (XRD) (measurement conditions: tube flow: 40 mA; tube pressure: 40 kV; wavelength (A): 0.15418 nm; scanning range: 5°~80°; scanning speed: 0.1 sec/step; scanning step size: 0.02°). The surface morphology and the composition of metal in the samples were studied through the scanning electron microscope (SEM) (measurement conditions: SE resolution: 3.0 nm (high vacuum, 30 kV), 10 nm (high vacuum, 3 KV); BSE resolution: 4.0 nm (low vacuum, 30 KV); multiplier: 5–300,000 times) along with the transmission electron microscope (TEM) (measurement conditions: point resolution: 0.25 nm; line resolution: 0.102 nm; acceleration voltage: 80, 100, 160 and 200 KV; tilt angle (X/Y): ±42/ ± 30°). The molecular structure of the sample was explored with the assistance of Fourier transform infrared spectroscopy (FTIR) (measurement conditions: test interval: 400–4,000 cm^{-1}; scan number: 32; resolution: 4 cm^{-1}). X-ray photoelectron spectroscopy (XPS) was used for the surface chemical analysis of the sample (measurement conditions: X light source with monochromatic Al Kα was selected, the full spectrum scanning energy was 160 eV, and the binding energy was corrected by C 1 s (284.8 eV)). The study also measured the Brunauer-Emmett-Teller (BET) surface area with the application of the Micromeritics ASAP 2460 analyzer (measurement conditions: analysis adsorptive: N_2; analysis bath temp.: 77.350 K; equilibration interval: 3 s; sample density: 1.000 g/cm^3). The Zeta potential of the sample was measured by Zeta-sizer Nano ZSE.

Isothermal study

The isotherm adsorption experiments were carried out as follows: 24 mg of HMO was added to 100 mL Pb^{2+}, Cd^{2+} and Ni^{2+} solutions; the concentrations are designed as 20 to 160 mg/L, 10 to 60 mg/L, and 10 to 60 mg/L respectively. The mixed solution was stirred for 45 min with a magnetic agitator (150 rpm/min). During the reaction, the pH value

was 4.0 and the temperature was 298.15 K. After the reaction, the contents of Pb^{2+}, Cd^{2+} and Ni^{2+} were determined by AAS. The Langmuir isotherm model (2) and Freundlich isotherm model (3) were used to fit the data.

$$c_e/q_e = c_e/q_m + 1/(K_L \bullet q_m) \quad (2)$$

$$q_e = K_f \bullet c_e^{1/n} \quad (3)$$

C_e (mg/L) represents the concentration of ions in the solution at equilibrium. K_L (L/mg), K_f and n respectively represent the Langmuir adsorption constant, the Freundlich adsorption constant and the Freundlich index. q_e and q_m (mg/g) refers to the equilibrium and the maximum capacity in adsorption of unit HMO, respectively.

Kinetic adsorption experiment

The kinetic adsorption experiments were designed as follows: To 3 × 200 mL beakers was added 100 mL Pb^{2+}, Cd^{2+} and Ni^{2+} solutions with different concentrations (the initial concentrations were 100, 30 and 30 mg/L respectively), and then 24 mg HMO was added respectively. The mixed solution was stirred with a magnetic agitator (150 rpm/min) for 2 h at 298.15 K. The pH of the solution was kept at 4 during the reaction. The residual concentrations of the three ions were analyzed by AAS after sampling at intervals (0~120 min).

The data obtained from the kinetic adsorption experiment was fitted by models of the pseudo-first-order and pseudo-second-order, and the adsorption mechanism of HMO was further analyzed, as expressed in Equations (4) and (5) respectively.

$$q_t = q_e \bullet (1 - e^{-k_1 \bullet t}) \quad (4)$$

$$t/q_t = 1/(k_2 \bullet q_e^2) + t/q_e \quad (5)$$

$k_1(min^{-1})$ refers to the rate constant of pseudo-first-order adsorption, while k_2(g/(mg/min)) is the rate constant of the pseudo-second-order adsorption. q_e and q_t (mg/g) respectively represent the adsorption proportion of heavy metal ions unit of HMO under equilibrium situation and at any time.

Experiments for Pb^{2+}, Cd^{2+} and Ni^{2+} removal

100 mL of Pb^{2+}, Cd^{2+} and Ni^{2+} solutions (100, 30 and 30 mg/L respectively) were taken. The pH value was controlled at between 2.0 and 6.0, and the influence of pH value on removing the three ions was explored. 24 mg of HMO was added to the heavy metal solution, and then the mixture was stirred with a magnetic agitator (150 rpm/min) at a predetermined pH for 45 min. In order to explore the promotion effect of $KMnO_4$ on HMO, 3 mL of 2.0 mmol/L $KMnO_4$ was added to the heavy metal solution with different amounts of HMO that ranged from 18 to 72 mg. The reaction was stirred for 45 min with a magnetic agitator (150 rpm/min) at a pH of 4. All samples were filtered and the residual concentration of heavy metal ions was detected by AAS. The consumption of $KMnO_4$ was studied by UV-visible absorption spectroscopy.

Co-adsorption of Pb^{2+}, Cd^{2+} and Ni^{2+}

In the treatment of industrial wastewater, there are multiple heavy metal ions that coexist in the system at the same time, and their adsorption is much more complicated than a single system. Several heavy metal ions not only have a competitive adsorption effect, but may also have synergistic or antagonistic effects, thus affecting the adsorption efficiency. Therefore, it is of great significance to explore the co-adsorption between different heavy metal ions to treat heavy metal ions in industrial wastewater.

100 mL of the same concentration (30 mg/L) of Pb^{2+}, Cd^{2+} and Ni^{2+} mixed solution was taken, and 3 mL 2.0 mmol/L $KMnO_4$ was added to the mixed solutions with different doses of HMO which ranged from 1–12 mg. The reaction was kept at pH 4.0 and stirred with a magnetic agitator (150 rpm/min) for 45 min. All samples were filtered after the reaction, and the residual concentration of heavy metal ions was detected by AAS.

Regeneration and recycling of adsorbents

Acidified potassium permanganate solution and hydrochloric acid solution were used to regenerate HMO after adsorption of heavy metals. After adsorption, we discarded the supernatant. Then 60 mL 0.1 M HCl solution and 10% acidified potassium permanganate solution were added to HMO. The eluent and adsorbent were stirred (150 rpm/min) in a water bath pot for 3 h and then filtered.

The concentration of Pb^{2+}, Cd^{2+} and Ni^{2+} in the filtrate was measured by AAS, the desorption amount was calculated according to Equation (6), and then the desorption rate was calculated according to Equation (7). The filtered HMO was desorbed again, and the above operation was

repeated five times.

$$q_d = \frac{C_d V}{W} \tag{6}$$

$$Elution\ rate = \frac{q_d}{q_e} \tag{7}$$

C_d (mg/L) is the desorption concentration; V (L) is the desorption volume; W (g) is the mass of adsorbent; q_e (mg/g) is the average adsorption amount of adsorption agent.

The eluted HMO was washed repeatedly with deionized water, and the regeneration was completed when the conductivity of the supernatant was below 2.0 μS·cm^{-1}. The regenerated HMO was absorbed again, and the above operation was cycled five times.

Table 1 | Specific surface area and pore diameter of different HMO

Sample	BET (m^2/g)	BJH (nm)
HMO-a	99.1	14.3
HMO-b	76.3	15.4
HMO-c	65.8	18.8

Table 2 | Zeta potential of different HMO

Types of HMO	HMO-a	HMO-b	HMO-c
pH value	1.5 ± 0.1	3.5 ± 0.1	5.5 ± 0.1
Zeta potential (mV)	−54.3	−47.0	−40.6

RESULTS AND DISCUSSION

Characterization of HMO

It can be seen from Tables 1 and 2 that the pore diameters of the three HMOs were 10–20 nm, and they were all mesoporous materials. The higher the acidity, the higher the Zeta potential and the larger the specific surface area of the synthesized HMO. Among them, the Zeta potential (−54.3 mV) and specific surface area (99.1 m^2/g) of HMO-a were the largest, and the surface electrification and adsorption sites were also greatest.

According to Figure 1(a), HMO-a, HMO-b and HMO-c all showed characteristic peaks at 12.5°, 37° and 67.8°. Compared with the standard spectrum, the crystal type of the three materials were all δ-MnO_2 (JCPDS Card No.80-1098) (Nawaz *et al.* 2017). The XRD characteristic peak intensity and crystallinity of the three kinds of MnO_2 were low, and they were all amorphous MnO_2. Theoretically, the surface area and active site of manganese dioxide decrease sharply with the appearance of crystal forms. Since amorphous manganese dioxide is not limited by its crystal morphology, its adsorption performance is generally better (He 2011).

According to Figure 1(b), the peaks at 3,440 and 1,620 cm^{-1}, correspond with the stretch vibration and bending vibration of the O-H tape, respectively (Liu *et al.* 2001; Liu & Ooi 2003). The peak near 538 cm^{-1} is related to the stretch vibration of the Mn-O tape (Yang *et al.* 2004). The hydroxyl peak wave numbers of HMO-a and HMO-c were 3,440 and 3,419 cm^{-1}, respectively. With the increase of pH value, the stretching vibration peak of the hydroxyl group of HMOs occurred with red shift, which may be caused by the charging of the surface structure.

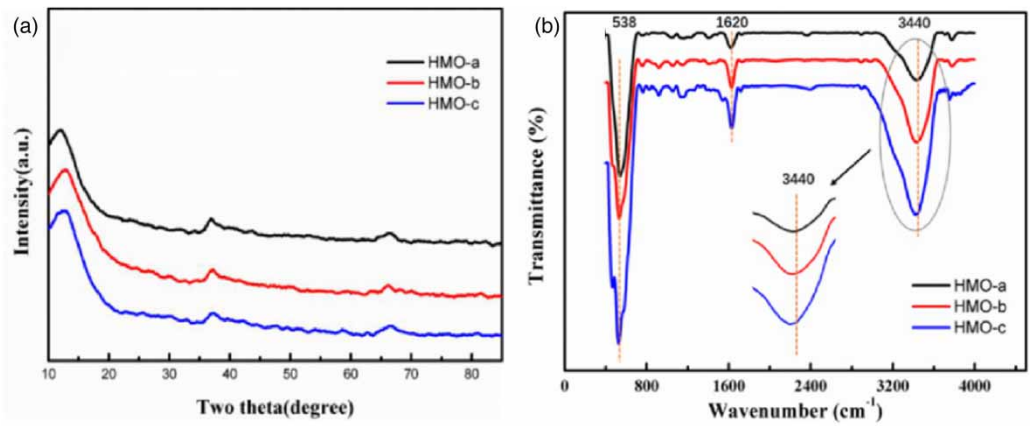

Figure 1 | (a) The XRD spectrum of different HMO, (b) The FTIR spectrum of different HMO.

The surface morphology of the synthesized HMO is significantly different at different pH (Figure S1, Supplementary Materials). The surface texture of HMO-a is obvious, showing a petal-like structure; the surface texture of HMO-b becomes shallow and the petal structure gradually decreases, while HMO-c presents a relatively smooth spherical shape. Among them, HMO-a has better particle dispersibility than HMO-b and HMO-c, and can provide more adsorption sites.

The micromorphology and size of HMO-a were analyzed. The surface morphology of HMO-a is presented in Figure 2(a). The element analysis of HMO-a is shown in Figure 2(b). The elements Mn and O were detected, as well as a small dose of the element K, which may come from the reactant $KMnO_4$. The TEM images (Figure 2(c)) confirmed that the HMO sample had a flower-like spherical structure with a diameter of about 300 nm. The application of a high-angle dark field scanning transmission electron microscope (Figure 2(d)) along with the use of elemental mapping images (Figure 2(e) and 2(f)) revealed that the elements of Mn (red zone) and O (green zone) were homogeneously dispersed throughout the whole material.

Adsorption study on the HMO

Effects of different HMO on adsorption

As can be seen from Figure S2, HMO-a has the best adsorption performance. Therefore, we chose HMO-a in the following experiments.

Effect of pH and HMO dosage

Figure 3(a) presents the influence of pH on the removal of Pb^{2+}, Cd^{2+} and Ni^{2+}. With the increase of pH, the removal rates of three metal ions all increased. At pH 6.0, the removal rates of three metal ions all reached the maximum values, which were 99.95%, 99.92% and 97.71%, respectively. When the pH value of the solution is higher than 4.0, Pb^{2+} will form a precipitate, so we conducted the following experiments at pH 4.0.

Besides, the influence of HMO dosage on the adsorption capacity and the removal rate of each metal ion is presented in Figure 3(b)–3(d). As the HMO dosage increased from 12 to 60 mg, the removal rate of Pb^{2+} and Cd^{2+} also increased from 67.91% to 99.99% and 84.83% to 99.97%, respectively. For Ni^{2+} solution, the result increased from 38.80% to 98.91%. After HMO treatment, the residual concentrations of Pb^{2+} and Cd^{2+} were under 0.01 mg/L, indicating that HMO has great potential in the treatment of heavy metal polluted water. As the dosage of HMO increases, the adsorption capacity of metal ions dropped sharply. When the dosage of HMO was 12 mg, the adsorption capacities of Pb^{2+}, Cd^{2+} and Ni^{2+} were 565.9, 212.08 and 97.08 mg/g respectively. When the dosage of HMO increased to 60 mg, the adsorption capacities decreased to 166.63, 49.98 and 49.45 mg/g, respectively. The increase of HMO dosage provided more active sites and surface areas for the solute, leading to the gradual increase of removal rate. Since there are still many

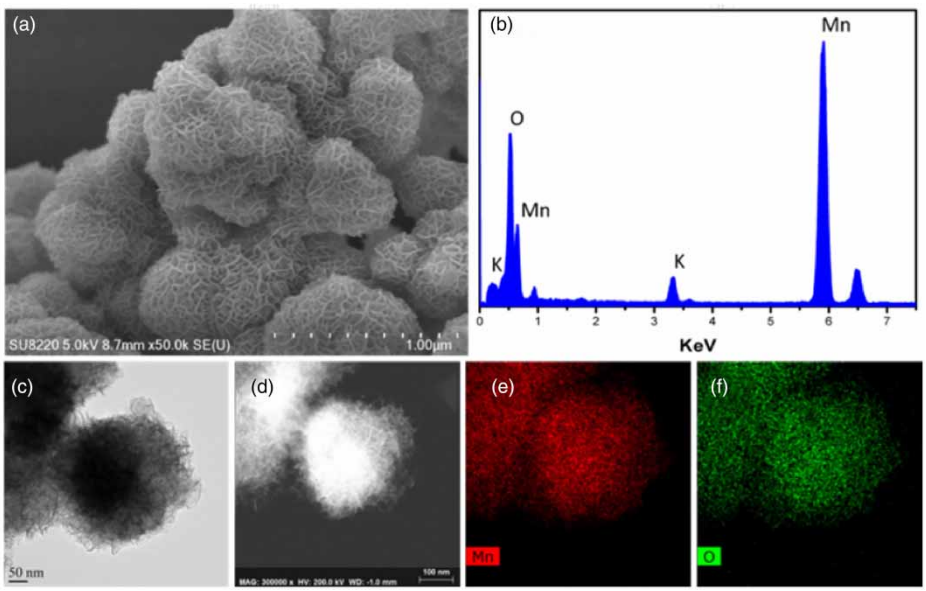

Figure 2 | Morphologies of HMO-a: (a) SEM image of HMO-a; (b) the corresponding EDS spectrum of HMO-a; (c) TEM image of HMO-a; (d) HAADF-STEM image of HMO-a; (e,f) TEM image and the corresponding EDS mapping; Mn (red zone), O (green zone).

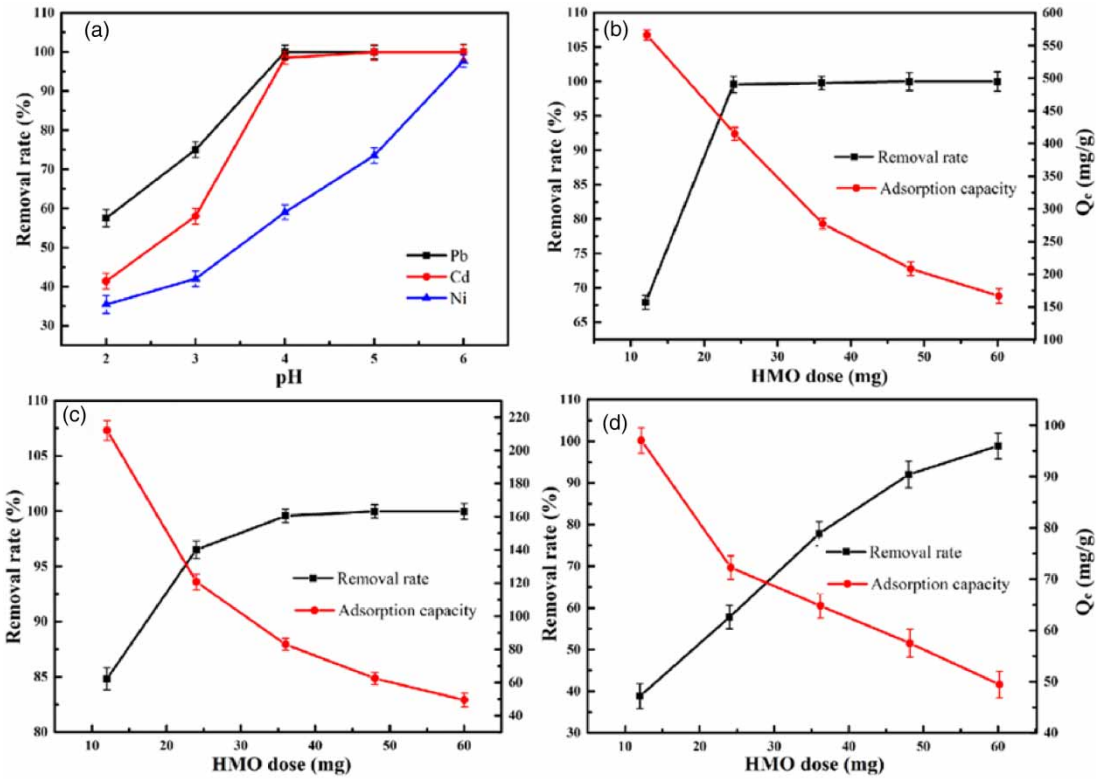

Figure 3 | (a) Effect of pH on Pb (II), Cd (II) and Ni (II) removal; effect of HMO dosage on (b) Pb (II), (c) Cd (II), and (d) Ni (II) removal.

active sites on the surface of the large doses of HMO adsorbents after the first heavy metal adsorption, the adsorption amount per unit mass of adsorbents will decrease sharply. Therefore, the improvement of the adsorption efficiency of HMO and reduction in the amount of HMO is of significant importance.

Effect of $KMnO_4$ on the removal of heavy metal ions

The effect of the combination of $KMnO_4$ and HMO on the depth removal of Pb^{2+}, Cd^{2+} and Ni^{2+} is expressed in Figure 4. When the residual concentrations of Pb^{2+}, Cd^{2+} and Ni^{2+} were respectively below 0.02, 0.01 and 0.02 mg/L, the minimum doses of HMO without the addition of $KMnO_4$ were 42, 54 and 78 mg, respectively. After adding $KMnO_4$, the minimum dose of HMO was reduced to 30, 36 and 66 mg, respectively, and the residual concentration met class II, V, and I surface water standards in China, respectively. The residual concentration of Mn (II) is below 0.01 mg/L, which meets the class I surface water standard in China. Therefore, the promotion effect of $KMnO_4$ significantly reduced the amount of adsorbent HMO, and the combined treatment method has a high removal rate and a good prospect for industrial application.

Study on co-adsorption

As shown in Figure 5, HMO has the strongest affinity for Pb^{2+}. When the dose of HMO is small, Pb^{2+} is first adsorbed. Among them, the removal rate of Ni^{2+} increased most slowly indicating that the adsorption capacity of HMO for Ni^{2+} was relatively low. The co-adsorption capacity of HMO for heavy metal ions is $Pb^{2+} > Cd^{2+} > Ni^{2+}$, which corresponds to the experimental results for single heavy metal ions.

The difference in adsorption capacity for different heavy metal ions is related to the effective radius of hydration ions and the first-order hydrolysis constant. The smaller the ionic hydration radius, the easier for the adsorbate to approach the adsorption potential of the HMO surface. The effective hydration radius of heavy metal ions in aqueous solution is $Pb^{2+} < Cd^{2+} < Ni^{2+}$, so Pb^{2+} has the strongest affinity with HMO. Studies have shown that the reduction of the average charge of ions can reduce the capacity barrier in

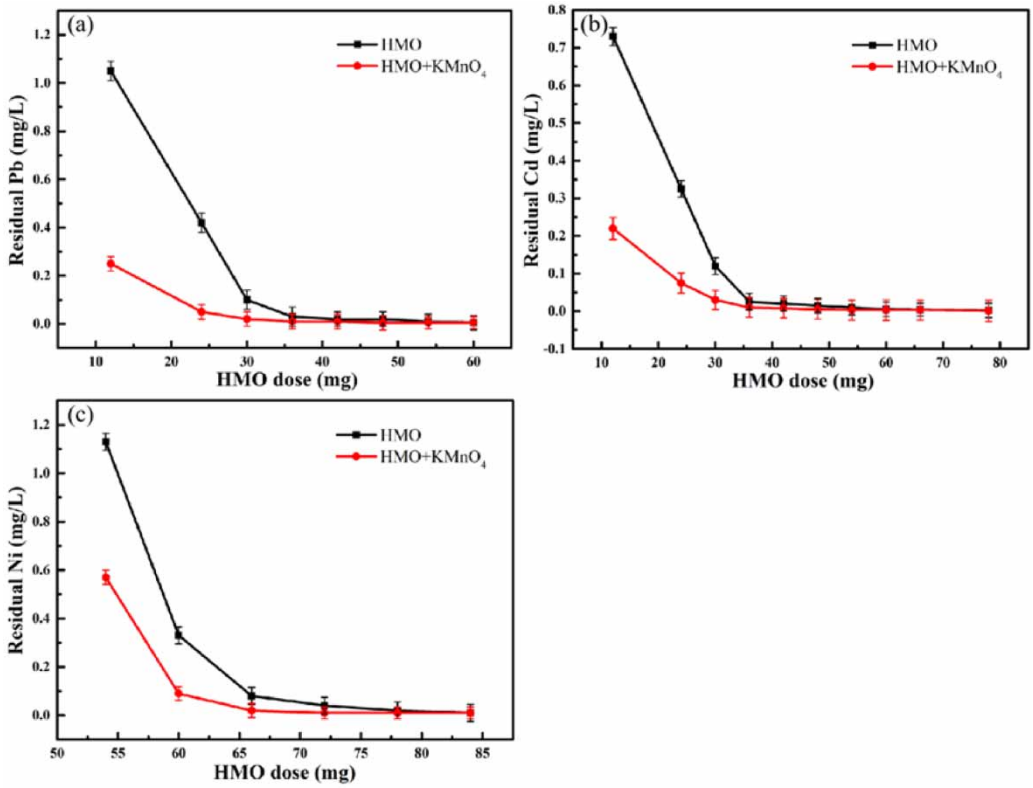

Figure 4 | The depth removal of (a) Pb (II), (b) Cd (II) and (c) Ni (II) with HMO combined with $KMnO_4$.

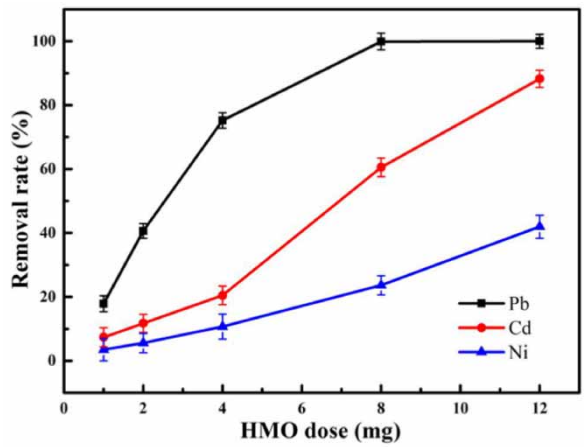

Figure 5 | Effect of co-existing heavy metal ions on heavy metal removal.

the adsorption process, which is conducive to the adsorption of metal ions on the oxide surface under the action of intermolecular force and electrostatic attraction, and the adsorption amount of hydrolysate or hydroxyl complex is greater than that of heavy metal ions. Because Pb^{2+} has a larger first-order hydrolysis constant, there are relatively more $PbOH^+$ in the water, so Pb^{2+} has a larger adsorption capacity (Zhang *et al.* 2008; Naiya *et al.* 2009). In the case of a small amount of HMO, although HMO shows a high adsorption selectivity for Pb^{2+}, it also has a certain adsorption capacity for other heavy metal ions, indicating that there may be obligate adsorption sites on the surface of HMO (Zhang *et al.* 2008). Besides, some studies have shown that when HMO adsorbs heavy metal ions, Mn^{2+} is released, and the amount of release is related to the type of metal ions (Naiya *et al.* 2009).

Adsorption isotherm

The data obtained from the isotherm adsorption experiment was fitted by the Langmuir model and the Freundlich model (Figure 6), and the parameters are listed in Table S1 (Supplementary Materials). As the equilibrium concentration of heavy metal ions gradually increases, the adsorption of Pb^{2+}, Cd^{2+} and Ni^{2+} by HMO also increases, rapidly at first, and then slowly to the equilibrium adsorption amount. At 303.15 K, the maximum adsorption equilibrium capacities (Q_m) of Pb^{2+}, Cd^{2+} and Ni^{2+} by HMO reached 541.70, 145.65 and 78.30 mg/g respectively. The ability of HMO to remove Pb, Cd and Ni decreases successively.

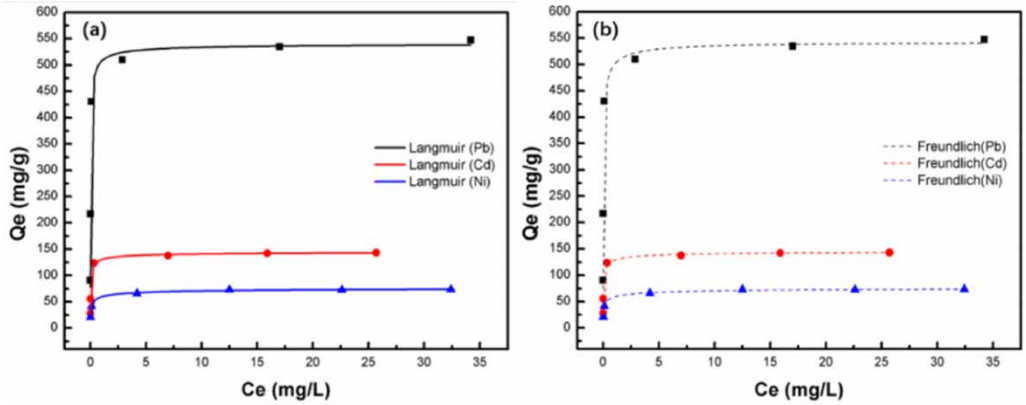

Figure 6 | Adsorption isotherms of Pb (II), Cd (II) and Ni (II) onto HMO at pH 4.0 and 298.15 K.

The adsorption correlation coefficient (R^2) of Pb^{2+}, Cd^{2+} and Ni^{2+} by HMO fitted by the Langmuir model is 0.9923~0.9962 and relative error (δ) is −0.37~6.17, which is more accurate than that fitted by the Freundlich model (R^2: 0.9840~0.9871, δ: −2.61~6.87). Moreover, the maximum adsorption capacity (Q_m) and equilibrium adsorption capacity (Q_e) obtained by the Langmuir model fitting isotherm adsorption experiment data are not significantly different, which further indicates that the Langmuir model is more accurate in fitting the isotherm adsorption experimental data, which also means that the adsorption of Pb^{2+}, Cd^{2+} and Ni^{2+} on the HMO surface is a single molecule adsorption. The HMO surface active sites were evenly distributed. The Langmuir adsorption constants (K_L): Pb^{2+}> Cd^{2+}> Ni^{2+} also indicated that the removal ability of HMO for Pb, Cd and Ni decreases successively. Table S2 shows the maximum adsorption capacities on HMO in our manuscript and other reported adsorbents. The HMO studied in this paper has excellent adsorption properties for Pb^{2+}, Cd^{2+} and Ni^{2+}, and is superior to most other expensive composite adsorbent materials.

Adsorption kinetics

The adsorption kinetic experiment was conducted to further explore the relationship between contact time and adsorption amount, to explore the mechanism further. The data were fitted by models of the pseudo-first and pseudo-second order (Figure 7), and the parameters are listed in Table S3. The adsorption capacity increased sharply in the first 5 mins, then continued to increase at a slower pace, and reached adsorption equilibrium at the point of 10 min, over 20 min, adsorption was in dynamic equilibrium. In this experiment, the adsorption equilibrium time was much shorter than most other adsorbents (Burakov *et al.* 2018). This indicates that the adsorption rate of Pb^{2+}, Cd^{2+} and Ni^{2+} by HMO is very fast, which can greatly improve the

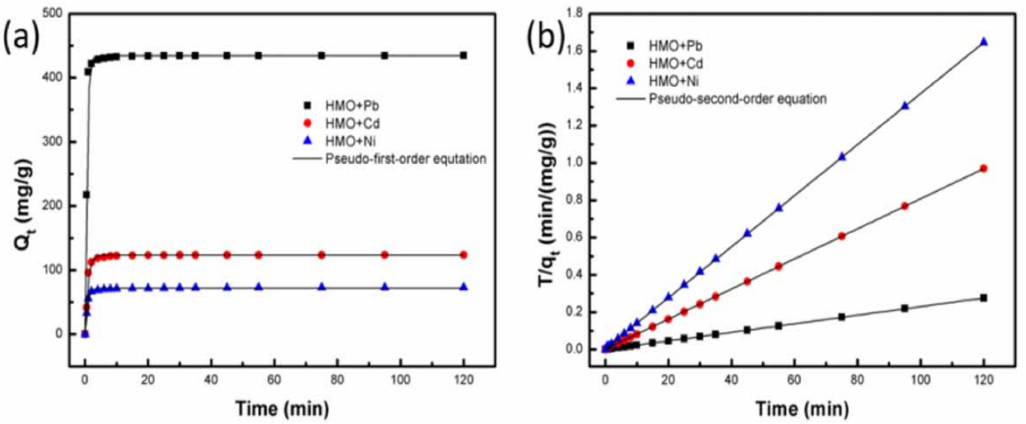

Figure 7 | Pseudo-first-order and Pseudo-second-order of Pb (II), Cd (II) and Ni (II) adsorption onto HMO at pH 4.0 and 298.15 K.

efficiency of industrial application. The fitting results showed that the correlation coefficient R_2^2(0.9999) and relative error δ_2 (0.04~−0.33) were more accurate than that R_1^2(0.98~0.99) and δ_1 (−1.53~−0.03). The pseudo-first-order adsorption kinetic model is mainly used to describe the physical adsorption process. The pseudo-second-order adsorption kinetic model with high fitting degree indicated that the adsorption process of Pb^{2+}, Cd^{2+} and Ni^{2+} by HMO had multiple adsorption stages. The adsorption process is not only affected by its characteristics, but also affected by the active sites on the surface of the adsorbent, electrostatic force and other factors, chemical adsorption and physical adsorption coexist, of which chemical adsorption is dominant (He & Xie 2018).

Regeneration research

The elution rate of HMO after adsorption of Pb^{2+}, Cd^{2+} and Ni^{2+} are listed in Table S4, the desorption rate of potassium permanganate eluent is higher than that of hydrochloric acid eluent. As can be seen from Figure 8, after 5 cycles of adsorption, the removal rates of Pb^{2+}, Cd^{2+} and Ni^{2+} with potassium permanganate as the desorption agent were 79.25%, 80.13% and 60.43%, respectively, which still maintained a high removal rate. The removal rate of Pb^{2+}, Cd^{2+} and Ni^{2+} with hydrochloric acid as the desorption agent decreased to 61.02%, 61.36% and 45.9%, respectively. This indicates that compared with hydrochloric acid, using acid $KMnO_4$ as the desorption agent to regenerated HMO-a can improve the cyclic removal rate of heavy metal ions. Therefore, it has a great prospect for development in industrial application.

Mechanism of the metal removal with $KMnO_4$

The role of $KMnO_4$ in heavy metal ion removal was explored by a series of characterizations. Figure S3 shows the FTIR spectrum comparison of HMO before and after the adsorption of Pb^{2+}, Ni^{2+} and Cd^{2+}. After adsorption of Pb^{2+}, Ni^{2+} and Cd^{2+}, the hydroxyl groups at 3,440 cm^{-1} began to significantly shift to 3,437, 3,435 and 3,430 cm^{-1}. The peaks at 1,395 and 2,083 cm^{-1} may indicate the existence of metallic hydroxyl or metallic oxides (Zhang & Li 2017). This proves that the adsorption process can be regarded as the interaction activity between the O-H groups of HMO and heavy metal ions (Xiong *et al.* 2011).

The TEM images (Figure 9) showed that the flower-like spherical structure of HMO remained unchanged after the reaction. The elemental mapping revealed that Mn, O and heavy metal (Pb, Cd, and Ni) elements were homogeneously dispersed throughout the HMO. This indicates that our material can uniformly adsorb heavy metal ions, and its morphology remains unchanged, which proves that our material can be fully utilized.

The XPS full spectrum is shown in Figure S4. There were obvious peaks near 285, 535 and 640 eV in the scanning spectra before and after HMO adsorption, which were Mn 3 s, C 1 s, O 1 s and Mn 2p peaks respectively. C 1 s is used as the standard peak to adjust the position of other peaks. The absorption peaks of Pb, Cd and Ni appeared in the XPS scanning spectra of HMO after adsorption of Pb^{2+}, Cd^{2+} and Ni^{2+}.

Figure S5 shows the narrow scanning area of Mn 2p before and after adsorption of Pb^{2+}, Cd^{2+} and Ni^{2+}. It can be observed that Mn 2p has two main peaks, the positions of which are Mn $2p_{3/2}$ of 642.52 eV and Mn $2p_{1/2}$ of

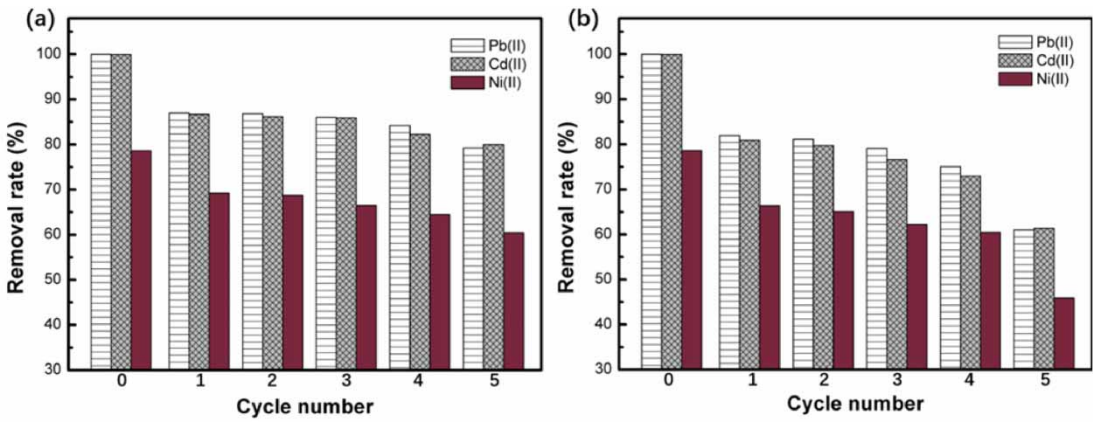

Figure 8 | Heavy metal removal rate of HMO-a in successive cycles: desorption agent (a) $KMnO_4$, (b) HCl.

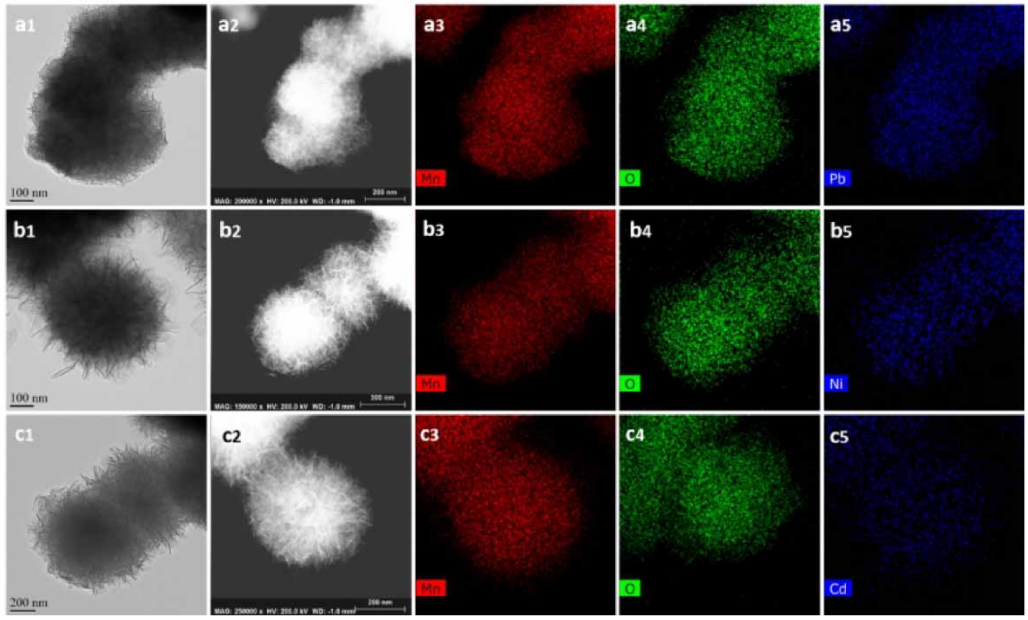

Figure 9 | TEM image of HMO after adsorption of (a_1) Pb(II), (b_1) Ni(II), and (c_1) Cd(II); (a_2) ~ (c_2) HAADF-STEM image of HMO after adsorption of (a_2) Pb (II), (b_2) Ni (II), and (c_2) Cd (II); the corresponding EDS mapping of HMO after adsorption of (a_3-a_5) Pb (II), (b3-b5 Ni (II), and (c3-c5) Cd (II).

654.33 eV respectively, indicating that HMO mainly existed in the form of MnO_2. After adsorption, the two main peaks did not deviate from each other, but the peak shape was weakened, possibly due to the effect of adsorption of heavy metal. The results show that the combined state of Mn in HMO did not change basically before and after adsorption.

Figure S6 shows the narrow scanning area of O 1 s before and after the adsorption of heavy metal ions by HMO. There are three chemical states of oxygen in HMO, namely hydroxyl oxygen (OH^-), lattice oxygen (O^{2-}) and oxygen in H_2O (Peng *et al.* 2015). Since the electronegativity of H is greater than that of Mn, the density of the surrounding electron cloud after the combination of O and H is smaller than that after the combination of O and Mn, and the inner electrons are reduced by the shielding effect of the outer electrons and strengthened by the binding effect of the electron nucleus. Therefore, the binding energy of inner electrons increases, in which the binding energy of oxygen in H_2O is the highest, followed by hydroxyl oxygen (OH^-), and lattice oxygen (O^{2-}) is the lowest (Pan *et al.* 2010). Figure S6a shows HMO without heavy metal adsorption. The binding energies of lattice oxygen (O^{2-}), hydroxyl oxygen (OH^-) and oxygen in H_2O are 530.14 eV, 532.20 eV and 533.74 eV, respectively, which is consistent with the research.

The relative contents of different forms of O on the HMO surface before and after the absorption of heavy metals are shown in Table S5. The binding energies of the characteristic peaks of O 1 s were all changed after adsorption. The binding energies are related to the density of electron clouds around O, indicating that heavy metal ions Pb^{2+}, Cd^{2+} and Ni^{2+} chemically bond with the O atoms of the hydroxyl group and bind to the surface of HMO in the form of coordination. The metal oxide content increased significantly, from 37.72 to 66.32, 62.01 and 74.57%, respectively, confirming Ni-O, Cd-O and Pb-O bonds were formed. The surface hydroxyl content decreased significantly, from 47.25 to 22.36, 21.90 and 20.26%, proving that the adsorption of Cd^{2+}, Ni^{2+} and Pb^{2+} has a correlation relationship with the surface hydroxyl groups. Due to the electronegativity of the HMO surface, Pb^{2+}, Ni^{2+} and Cd^{2+} will bind to hydroxyl groups on the surface of HMO by coordination bonds, and the protons of hydroxyl groups are dissociated and exchanged with Pb^{2+}, Ni^{2+} and Cd^{2+}, part of Pb, Ni and Cd exist in the form of hydroxide complexes $PbOH^+$, $NiOH^+$ and $CdOH^+$, and bind to the hydroxyl groups on the surface of HMO in the form of the hydroxide complex.

Figure S7 shows the narrow scanning area after the adsorption of three heavy metal ions. The peaks located at 405.2 and 411.9 eV were Cd $3d_{5/2}$ and Cd $3d_{3/2}$ (Figure S7a). Cd $3d_{5/2}$ and Cd $3d_{3/2}$ are basically symmetrical with high peak intensity. Such a peak pattern indicates that Cd is in a single substance state on the surface of HMO. By comparing the peak value of 405 eV corresponding to Cd $3d_{5/2}$ in the literature, it can be determined that Cd on the surface is in a CdO state (Tkachenko *et al.* 1993). The

two peaks of 855.5 and 870.7 eV in Figure S7b are Ni $2p_{3/2}$ and Ni $2p_{1/2}$, which corresponds with the reported value for the NiO state (Salvati *et al.* 1981). The XPS spectrum of Pb 4f presents two distinct peaks, located at 137.8 eV and 142.6 eV (Figure S7c), deriving from Pb $4f_{7/2}$ and Pb $4f_{5/2}$, respectively. The bond energies of Pb $4f_{7/2}$ of PbO are known to range from 137.6 eV to 138.2 eV (Naiya *et al.* 2009), so it can be determined that Pb on the surface is in a PbO state. The shape of the peaks indicates the valence state of Cd, Ni and Pb on HMO is +2 valence, which means they were not oxidized in the process of adsorption with the existence of $KMnO_4$.

The variation trend of $KMnO_4$ in the reaction process was observed by UV-Vis spectrum. Each curve contains a main peak. The peak at 525 nm is the maximum absorption wavelength of $KMnO_4$, and the consumption of $KMnO_4$ can also be detected from the change of the absorbance in the curve. HMO and $KMnO_4$ were stirred in 100 mL deionized water with a pH of 4 for 45 min, and the spectrum before and after stirring is shown in Figure S8a. It can be observed that the two curves almost completely coincide, indicating that $KMnO_4$ was not decomposed during the stirring process; that is, $KMnO_4$ did not react with HMO. However, when the deionized water was replaced by the same volume of Pb^{2+}, Cd^{2+} and Ni^{2+} solutions, $KMnO_4$ was detected to be consumed (Figure S8b, S8c, and S8d). When the dosages of HMO applied differed in the adsorption of heavy metal ions, the consumed volume of $KMnO_4$ varied too. The more HMO was added, the more $KMnO_4$ was consumed. Figure S8e shows the variation of $KMnO_4$ absorbance with time when HMO adsorbs Pb^{2+}. About 50% of $KMnO_4$ was consumed when the reaction lasted for five minutes, and the absorbance of $KMnO_4$ decreased gradually as the adsorption reaction proceeded.

Combined with the analysis results of XPS, the valence state of heavy metals did not change during the adsorption process, indicating that $KMnO_4$ did not react with the low-state heavy metal ions during the adsorption process, further indicating that only the presence of heavy metal ions in the system can cause the consumption of $KMnO_4$. Naiya *et al.* (2009) found that when HMO adsorbed heavy metal ions, a small amount of Mn^{2+} was released, and the consumed $KMnO_4$ in the solution was likely to react with the free Mn^{2+} in the solution. We did experiments to test this hypothesis: 24 mg HMO was added to 100 mL of deionized water and stirred for 45 min at a pH of 4. At this time, the concentration of Mn^{2+} in the supernatant was less than 0.01 mg /L. When 100 mL 100 mg/L Pb^{2+} solution was used instead of deionized water, the residual concentration of Mn^{2+} increased sharply to 4.85 mg/L after the adsorption was completed. However, after adding 3 mL 2.0 mmol/L $KMnO_4$ into the Pb^{2+} solution, the residue of Mn^{2+} was reduced to below 0.01 mg/L again. The molar ratio of Mn^{2+} released and $KMnO_4$ consumed during the reaction is roughly consistent with Equation (1). It can be inferred that there are +2 valence Mn elements on the surface of HMO crystal or between layers. When the heavy metals are adsorbed, Mn^{2+} is released, and the released Mn^{2+} reacts with $KMnO_4$ in the solution to form a small amount of in-situ HMO. In-situ HMO has high activity and strong adsorption capacity, which can effectively improve the removal efficiency of heavy metal ions in the solution.

CONCLUSIONS

The HMO synthesized at low pH value with the flower-like spherical structure was an effective environmental material to remove Pb^{2+}, Cd^{2+} and Ni^{2+} in solutions. At 298.15 K and pH 4.0, the Langmuir isotherm model was well adapted to the experimental results, and the maximum adsorption capacities were 541.70, 145.65 and 78.30 mg/g, respectively. The adsorption of heavy metals by HMO belongs to monomolecular adsorption and the adsorption process is mainly controlled by chemisorption. After adsorption, the heavy metal ions coordinate with the HMO groups, and the HMO morphology remains unchanged after adsorption. Mn^{2+} will be released when HMO adsorbs metal ions, resulting in Mn^{2+} pollution. The 'HMO + $KMnO_4$' system can not only remove the released Mn^{2+} through the redox reaction, but also generate highly active in-situ HMO, which improves the removal efficiency. The co-adsorption capacity of HMO for heavy metal ions is Pb^{2+}> Cd^{2+}> Ni^{2+}. Pb^{2+} has a smaller hydration radius and a larger first-order hydrolysis constant, so Pb^{2+} has the strongest affinity with HMO. Regeneration of adsorbents can avoid the waste of resources and secondary pollution caused by discarded adsorbents. The regeneration ability of acidic potassium permanganate to HMO was higher than that of hydrochloric acid. After 5 cycles of adsorption, HMO still maintained a high adsorption rate.

ACKNOWLEDGEMENT

This work was supported by the Department of Environmental Protection of Guangdong Province under Grant number B2152990.

CONFLICTS OF INTEREST

The authors declare no conflicts of interest.

DATA AVAILABILITY STATEMENT

All relevant data are included in the paper or its Supplementary Information.

REFERENCES

Burakov, A. E., Galunin, E. V., Burakova, I. V., Kucherova, A. E., Agarwal, S., Tkachev, A. G. & Gupta, V. K. 2018 Adsorption of heavy metals on conventional and nanostructured materials for wastewater treatment purposes: a review. *Ecotoxicology and Environmental Safety* **148**, 702–712. doi:10.1016/j.ecoenv.2017.11.034.

Gadd, G. M. 2009 Biosorption: critical review of scientific rationale, environmental importance and significance for pollution treatment. *Journal of Chemical Technology and Biotechnology* **84** (1), 13–28. doi:10.1002/jctb.1999.

Hashim, M. A., Mukhopadhyay, S., Sahu, J. N. & Sengupta, B. 2011 Remediation technologies for heavy metal contaminated groundwater. *Journal of Environmental Management* **92** (10), 2355–2388. doi:10.1016/j.jenvman.2011.06.009.

He, J. J. 2011 Preparation of MnO_2/Fe_3O_4 composite adsorbent and study on the adsorption of lead and copper in water. *Harbin Institute of Technology*. MD thesis, Harbin, China. doi:10.7666/d.D260051.

He, C. & Xie, F. 2018 Adsorption behavior of manganese dioxide towards heavy metal ions: surface zeta potential effect. *Water Air and Soil Pollution* **229**, 3. doi:10.1007/s11270-018-3712-6.

Hua, M., Zhang, S., Pan, B., Zhang, W., Lv, L. & Zhang, Q. 2012 Heavy metal removal from water/wastewater by nanosized metal oxides: a review. *Journal of Hazardous Materials* **211**, 317–331. doi:10.1016/j.jhazmat.2011.10.016.

Li, S. Q., Chen, Y. F., Pei, X. K., Zhang, S. H., Feng, X., Zhou, J. W. & Wang, B. 2016 Water purification: adsorption over metal-organic frameworks. *Chinese Journal of Chemistry* **34** (2), 175–185. doi:10.1002/cjoc.201500761.

Liu, Z. H. & Ooi, K. 2003 Preparation and alkali-metal ion extraction/insertion reactions with nanofibrous manganese oxide having 2×4 tunnel structure. *Chemistry of Materials* **15** (19), 3696–3703. doi:10.1021/cm030344z.

Liu, Z. H., Ooi, K., Kanoh, H., Tang, W. P., Yang, X. J. & Tomida, T. 2001 Synthesis of thermally stable silica-pillared layered manganese oxide by an intercalation/solvothermal reaction. *Chemistry of Materials* **13** (2), 473–478. doi:10.1021/cm000633c.

Lyu, S., Chen, W., Zhang, W., Fan, Y. & Jiao, W. 2016 Wastewater reclamation and reuse in China: opportunities and challenges. *Journal of Environmental Sciences* **39**, 86–96. doi:10.1016/j.jes.2015.11.012.

Mezohegyi, G., van der Zee, F. P., Font, J., Fortuny, A. & Fabregat, A. 2012 Towards advanced aqueous dye removal processes: a short review on the versatile role of activated carbon. *Journal of Environmental Management* **102**, 148–164. doi:10.1016/j.jenvman.2012.02.021.

Naiya, T. K., Bhattacharya, A. K. & Das, S. K. 2009 Adsorption of Cd(II) and Pb(II) from aqueous solutions on activated alumina. *Journal of Colloid and Interface Science* **331** (1), 14–26. doi:10.1016/j.jcis.2009.01.003.

Nawaz, F., Cao, H., Xie, Y., Xiao, J., Chen, Y. & Ghazi, Z. A. 2017 Selection of active phase of MnO_2 for catalytic ozonation of 4-nitrophenol. *Chemosphere* **168**, 1457–1466. doi:10.1016/j.apcatb.2017.02.068.

Ojedokun, A. T. & Bello, O. S. 2016 Sequestering heavy metals from wastewater using cow dung. *Water Resources and Industry* **13**, 7–13. doi:10.1016/j.wri.2016.02.002.

Otrembska, P. & Gega, J. 2012 Separation of nickel(II) and cadmium(II) with ion-exchange process. *Separation Science and Technology* **47** (9), 1345–1349. doi:10.1080/01496395.2012.672520.

Pan, B., Qiu, H., Pan, B., Nie, G., Xiao, L., Lv, L., Zhang, W., Zhang, Q. & Zheng, S. 2010 Highly efficient removal of heavy metals by polymer-supported nanosized hydrated Fe(III) oxides: behavior and XPS study. *Water Research* **44** (3), 815–824. doi:10.1016/j.watres.2009.10.027.

Patil, D. S., Chavan, S. M. & Kennedy Oubagaranadin, J. U. 2016 A review of technologies for manganese removal from wastewaters. *Journal of Environmental Chemical Engineering (Netherlands)* **4** (1), 468–487. doi:10.1016/j.jece.2015.11.028.

Peng, L., Zeng, Q., Tie, B., Lei, M., Yang, J., Luo, S. & Song, Z. 2015 Manganese dioxide nanosheet suspension: a novel absorbent for Cadmium(II) contamination in waterbody. *Journal of Colloid and Interface Science* **456**, 108–115. doi:10.1016/j.jcis.2015.06.017.

Salvati, L., Makovsky, L. E., Stencel, J. M., Brown, F. R. & Hercules, D. M. 1981 Surface spectroscopic study of tungsten-alumina catalysts using x-ray photoelectron, ion scattering, and Raman spectroscopies. *Journal of Physical Chemical* **85**, 3700–3707. doi:10.1021/j150624a035.

Sheela, T., Nayaka, Y. A., Viswanatha, R., Basavanna, S. & Venkatesha, T. G. 2012 Kinetics and thermodynamics studies on the adsorption of Zn(II), Cd(II) and Hg(II) from aqueous solution using zinc oxide nanoparticles. *Powder Technology* **217**, 163–170. doi:10.1016/j.powtec.2011.10.023.

Su, Q., Pan, B. C., Pan, B. J., Zhang, Q. R., Zhang, W. M., Lv, L., Wang, X. S., Wu, J. & Zhang, Q. X. 2009 Fabrication of polymer-supported nanosized hydrous manganese dioxide (HMO) for enhanced lead removal from waters. *Science of the Total Environment* **407** (21), 5471–5477. doi:10.1016/j.scitotenv.2009.06.045.

Su, Q., Pan, B., Wan, S., Zhang, W. & Lv, L. 2010 Use of hydrous manganese dioxide as a potential sorbent for selective removal of lead, cadmium, and zinc ions from water. *Journal of Colloid and Interface Science* **349** (2), 607–612. doi:10.1016/j.jcis.2010.05.052.

Sun, W. L., Xia, J. & Shan, Y. C. 2014 Comparison kinetics studies of Cu(II) adsorption by multi-walled carbon nanotubes in

homo and heterogeneous systems: effect of nano-SiO_2. *Chemical Engineering Journal* **250**, 119–127. doi:10.1016/j.cej.2014.03.094.

Tkachenko, O. P., Shpiro, E. S., Wark, M., Schulz-Ekloff, G. & Jaeger, N. I. 1993 X-ray photoelectron/X-ray excited auger electron spectroscopic study of highly dispersed semiconductor CdS and CdO species in zeolites. *Journal of the Chemical Society* **89**, 3987–3994. doi:10.1039/FT9938903987.

Trellu, C., Mousset, E., Pechaud, Y., Huguenot, D., van Hullebusch, E. D., Esposito, G. & Oturan, M. A. 2016 Removal of hydrophobic organic pollutants from soil washing/flushing solutions: a critical review. *Journal of Hazardous Materials* **306**, 149–174. doi:10.1016/j.jhazmat.2015.12.008.

Wongsasuluk, P., Chotpantarat, S., Siriwong, W. & Robson, M. 2014 Heavy metal contamination and human health risk assessment in drinking water from shallow groundwater wells in an agricultural area in Ubon Ratchathani province, Thailand. *Environmental Geochemistry and Health* **36** (1), 169–182. doi:10.1007/s10653-013-9537-8.

Xiong, L., Chen, C., Chen, Q. & Ni, J. 2011 Adsorption of Pb(II) and Cd(II) from aqueous solutions using titanate nanotubes prepared via hydrothermal method. *Journal of Hazardous Materials* **189** (3), 741–748. doi:10.1016/j.jhazmat.2011.03.006.

Yang, X. J., Makita, Y., Liu, Z. H., Sakane, K. & Ooi, K. 2004 Structural characterization of self-assembled MnO_2 nanosheets from birnessite manganese oxide single crystals. *Chemistry of Materials* **16** (26), 5581–5588. doi:10.1021/cm049025d.

Zhai, Y. & Wang, H. 2016 Kinetics and mechanism study on adsorption of cadmium by freshly synthesized hydrous manganese dioxide. *Desalination and Water Treatment* **57** (15), 6981–6990. doi:10.1080/19443994.2015.1014860.

Zhang, Y. & Li, Z. 2017 Heavy metals removal using hydrogel-supported nanosized hydrous ferric oxide: synthesis, characterization, and mechanism. *Science of the Total Environment* **580**, 776–786. doi:10.1016/j.scitotenv.2016.12.024.

Zhang, L., Ma, J. & Yu, M. 2008 The microtopography of manganese dioxide formed in situ and its adsorptive properties for organic micropollutants. *Solid State Sciences* **10** (2), 148–153. doi:10.1016/j.solidstatesciences.2007.08013.

First received 28 October 2020; accepted in revised form 11 March 2021. Available online 23 March 2021